Magnetization reversal driven by spin-polarized current in exchange-biased nanoscale spin valves

G. Finocchio,[1] I. N. Krivorotov,[2] L. Torres,[3] R. A. Buhrman,[4] D. C. Ralph,[4] and B. Azzerboni[1]
[1]*Dipartimento di Fisica della Materia e Tecnologie Fisiche Avanzate, University of Messina, Salita Sperone 31, 98166 Messina, Italy*
[2]*Department of Physics and Astronomy, University of California, Irvine, California 92697-4575, USA*
[3]*Departamento de Fisica Aplicada, Universidad de Salamanca, Plaza de la Merced s/n, 37008 Salamanca, Spain*
[4]*Cornell University, Ithaca, New York 14853-2501, USA*
(Received 10 April 2007; revised manuscript received 27 August 2007; published 5 November 2007)

We report micromagnetic simulations of current-driven magnetization reversal of the free-layer nanomagnet in $Ir_{20}Mn_{80}/Ni_{80}Fe_{20}/Cu/Ni_{80}Fe_{20}$ nanoscale spin valves for large current pulses and compare the results to experiments. Our simulations demonstrate that the mechanism of current-driven magnetization reversal in these samples can depend strongly on the equilibrium angle between the magnetizations of the pinned layer and the free layer of the spin valve. In the case of collinear equilibrium magnetizations, the reversal proceeds via nucleation of a vortex. However, even small misalignments of the magnetizations of the free and the pinned layers, on the order of 5°–10°, can result in magnetization reversal by a macrospinlike coherent precessional rotation. This result is in good agreement with recent experimental observations.

DOI: 10.1103/PhysRevB.76.174408 PACS number(s): 75.40.Mg, 75.75.+a

I. INTRODUCTION

A spin-polarized current flowing through a nanomagnet applies a torque to its magnetization and can induce either magnetization reversal or persistent precession of the magnetization.[1,2] Understanding the mechanisms by which a spin-transfer torque drives magnetization reversal is important from both fundamental and practical points of view. Fundamentally, a detailed understanding of spin torque may enable more-controlled studies of large-angle magnetization dynamics. From the practical point of view, spin-transfer torque is a candidate mechanism for writing information in the next generation of nonvolatile magnetoresistive random access memory (MRAM). A better understanding of spin-transfer-driven magnetic reversal may lead to reductions of the current densities required to induce reversal or increases in the switching speed and thus give guidance for optimizing MRAM elements.

Recently, two time-domain measurement techniques have been employed for studies of magnetization reversal in nanoscale spin valves. Time-resolved electrical measurements of spin-transfer-driven magnetization reversal in $130\times60\times4$ nm^3 elliptical thin-film $Ni_{80}Fe_{20}$ (Py) nanomagnets within $Ir_{20}Mn_{80}$/Py/Cu/Py exchange-biased spin valves[3] were in good qualitative agreement with a macrospin model of the current-driven magnetization reversal. Time-resolved x-ray magnetic circular dichroism imaging of spin-transfer-driven reversal in $150\times100\times2$ nm^3 elliptical $Co_{86}Fe_{14}$ sample[4] (differing from Ref. 3 by the absence of an exchange-biased pinned layer and also by having a much larger switching current, so that the Oersted field was more significant) showed reversal proceeding via a vortex nucleation, confirming the prediction of micromagnetic simulations for a similar system.[5] In this paper, we analyze what factors influence the crossover from quasimacrospin to vortex-mediated spin-transfer switching for large current pulses (currents significantly larger than the zero-temperature critical currents). We find that the existence of a nonzero equilibrium angle between the magnetizations of the free and pinned magnetic layers, induced by exchange biasing, is a key factor giving rise to the macrospinlike coherent precessional reversal. At zero temperature, this coherent reversal process significantly reduces the reversal time, relative to vortex-mediated switching. However, at temperatures exceeding a few kelvin, the reversal times of the two reversal mechanisms are found to be similar.

The paper is organized as follows. Section II describes the details of our numerical micromagnetic simulations and the parameters used. In Sec. III, we performed a theoretical study of the reversal processes in the spin-torque-driven reversal regime, including the dependence of the magnetization reversal process on the equilibrium offset angle between the free-layer and pinned-layer magnetizations. In addition, we examine the effects of nonidealities in the sample shape and present experimental data and simulations on the temperature dependence of the current-driven magnetization reversal. Conclusions are given in Sec. IV.

II. SIMULATION DETAILS

The system studied in this paper is a spin valve consisting of two 4 nm Py ferromagnetic layers separated by an 8 nm Cu spacer, etched to have a nanopillar structure with elliptical cross section (130×60 nm^2). One of the ferromagnetic layers (the pinned layer) is exchange biased by an underlayer of 8 nm of antiferromagnetic $Ir_{20}Mn_{80}$, and the other ferromagnetic layer (the free layer) is free to reorient in response to the spin-transfer torque.[3] In our micromagnetic simulations, we employ a Cartesian system of coordinates in which the major axis of the ellipse is the x axis and the in-plane minor axis is the y axis. The simulations have been performed by numerically solving the Landau-Lifshitz-Gilbert-Slonczewski (LLGS) equation,[6,7]

$$\frac{d\mathbf{m}}{d\tau} = -(\mathbf{m}\times\mathbf{h}_{eff}) + \alpha\mathbf{m}\times\frac{d\mathbf{m}}{d\tau} - \frac{g|\mu_B|j}{e\gamma_0 M_s^2 L_z}\varepsilon(\mathbf{m},\mathbf{m}_p)\mathbf{m}\times(\mathbf{m}\times\mathbf{m}_p), \quad (1)$$

where g is the gyromagnetic splitting factor, γ_0 is the gyro-

magnetic ratio, μ_B is the Bohr magneton, α is the Gilbert damping, j is the current density, L_z is the thickness of the free layer, e is the electron charge, $\mathbf{m}=\mathbf{M}/M_S$ is the normalized magnetization of the free layer, $\mathbf{m_p}=\mathbf{M_p}/M_S$ is the normalized magnetization of the pinned layer, M_S is the saturation magnetization, $d\tau=\gamma_0 M_S dt$ is the dimensionless time step, and $\varepsilon(\mathbf{m},\mathbf{m_p})$ characterizes the angular dependence of the Slonczewski spin torque term. By convention, positive current polarity corresponds to the electron flow from the free to the pinned layer of the spin valve. $\mathbf{h}_{\text{eff}}$ is the dimensionless effective field ($\mathbf{h}_{eff}=\mathbf{H}_{eff}/M_S$), $\mathbf{H}_{eff}$ is given by $\mathbf{H}_{eff}=\mathbf{H}_{exch}+\mathbf{H}_{ani}+\mathbf{H}_{ext}+\mathbf{H}_M+\mathbf{H}_{amp}+\mathbf{H}_{AF}$, where $\mathbf{H}_{exch}$, $\mathbf{H}_{ani}$, $\mathbf{H}_{ext}$, and $\mathbf{H}_M$ are the standard micromagnetic contributions from exchange, anisotropy, external, and demagnetizing fields, $\mathbf{H}_{amp}$ is the Oersted field due to the current, and $\mathbf{H}_{AF}$ is the magnetostatic coupling between the pinned and the free layer. We only consider the shape contribution to anisotropy because the magnetocrystalline anisotropy of Py is expected to be small. In order to calculate the Slonczewski spin torque term, we make an approximation that the composition of the spin valve layers is symmetric with respect to the midpoint of the Cu spacer. This allows us to use simplified forms for the current polarization function $\varepsilon(\mathbf{m},\mathbf{m}_p)$ and the normalized magnetoresistance $\varepsilon(\mathbf{m},\mathbf{m}_p)$ derived by Slonczewski for a symmetric spin valve structure,[8] $\varepsilon(\theta)=0.5P\Lambda^2/[1+\Lambda^2+(1-\Lambda^2)\cos(\theta)]$ and $r(\theta)=[1-\cos^2(\theta/2)]/[1+\chi\cos^2(\theta/2)]$, where θ is the angle between the magnetizations of the free and the pinned layers $[\mathbf{m}\cdot\mathbf{m}_p=\cos(\theta)]$, χ is the giant magnetoresistance (GMR) asymmetry parameter, P is the current spin-polarization factor, and $\Lambda^2=\chi+1$.[8] This approximation is reasonable because the spin-flip length in Py is short, so the presence of the antiferromagnetic $Ir_{20}Mn_{80}$ layer should have little effect on the spin torque acting on the free layer.

Using vector identities, we convert Eq. (1) to an equivalent form that we find to be more convenient for our calculations,

$$(1+\alpha^2)\frac{d\mathbf{m}}{d\tau} = -(\mathbf{m}\times\mathbf{h}_{eff}) - \alpha\mathbf{m}\times(\mathbf{m}\times\mathbf{h}_{eff}) - \frac{g|\mu_B|j}{e\gamma_0 M_s^2 L_z}\varepsilon(\mathbf{m},\mathbf{m}_p)[\mathbf{m}\times(\mathbf{m}\times\mathbf{m}_p) - \alpha(\mathbf{m}\times\mathbf{m}_p)]. \quad (2)$$

We used the following parameters in the simulations. The saturation magnetization of the Py, $M_S=645\times10^3$ A/m, was determined from superconducting quantum interference device magnetometry measurements of a continuous 4 nm film of Py sandwiched between two films of Cu and subjected to the same heat-treatment protocol, as experienced by the experimental device during its nanofabrication process. The Gilbert damping parameter $\alpha=0.025$ for these samples was measured by a time-domain technique described in Ref. 3. We employed the standard exchange strength for Py, $A=1.3\times10^{-11}$ J/m. The current (and thus the spin torque) step applied to the nanopillar had a rise time of 150 ps, increasing linearly from zero to the maximum value of current. The parameters $\chi=1.5$ and $P=0.38$ in the expression for spin torque were obtained by fitting to the experimentally measured ensemble-average switching time (see below) for both low-resistance (LR) $\rightarrow$ high-resistance (HR) and HR $\rightarrow$ LR switching transitions, as described in Sec. III.

Our micromagnetic simulations are based on a time-domain finite difference code which has been developed in the last ten years by our group (Messina-Salamanca).[7] In the work reported here, we use a computational time step of 28 fs, and tests performed with a time step of 20 fs gave the same results. We use a spatial discretization cell of $2.5\times2.5\times4.0$ nm^3; tests with a cell size of $2.0\times2.0\times2.0$ nm^3 gave very similar results, with switching time variations of less than 4%.

III. RESULTS AND DISCUSSION

In this section, we describe the results of our LLGS simulations of the current-induced magnetization reversal in $Ir_{20}Mn_{80}$/Py/Cu/Py nanoscale spin valves for large current pulses with the goal of elucidating the role of device-geometry parameters and temperature on the reversal processes. First, we study the effect of the pinned-layer magnetization direction at zero temperature and find that the variation of this angle can lead to qualitatively different reversal mechanisms. Second, we examine the role of shape imperfections of the nominally elliptical sample and find that realistic deviations from the ideal shape can significantly alter the reversal time. Finally, we examine the effect of temperature on the reversal process and compare the results of our micromagnetic simulations to time-resolved measurements of the current-induced magnetization reversal. Our simulations successfully reproduce all major features of the experimental data, including the macrospinlike precessional reversal of magnetization, dispersion of the switching times due to thermal fluctuations, and temperature-induced dephasing of the averaged magnetization precession during the reversal process.

We simulate the reversal processes for a number of pinned-layer magnetization directions ($\beta=0°$, 5°, 10°, 20°, and 30°). In experiment, β can be controlled by exchange biasing the pinned layer at an angle with respect to the easy axis of the free layer (e.g., in Ref. 3, β is approximately 30°). For each β, the two initial configurations of the free-layer magnetization (LR and HR) have been computed by solving the static LLG equation ($\mathbf{m}\times\mathbf{h}_{eff}=0$),[9] including the magnetostatic coupling with the pinned layer. We use the terms "low resistance" and "high resistance" rather than parallel and antiparallel because whenever $\beta\neq0°$, the static states of the free- and pinned-layer magnetizations are not collinear. We computed the critical currents (zero external field) as a function of β [0° ($I_{\text{HR}\rightarrow\text{LR}}=-1.60$ mA, $I_{\text{LR}\rightarrow\text{HR}}=2.45$ mA), 10° ($I_{\text{HR}\rightarrow\text{LR}}=-1.60$ mA, $I_{\text{LR}\rightarrow\text{HR}}=2.46$ mA), 20° ($I_{\text{HR}\rightarrow\text{LR}}=-1.44$ mA, $I_{\text{LR}\rightarrow\text{HR}}=2.58$ mA), 30° ($I_{\text{HR}\rightarrow\text{LR}}=-1.50$ mA, $I_{\text{LR}\rightarrow\text{HR}}=3.18$ mA)].

Figure 1 shows the temporal evolution of the x component of the free-layer magnetization during current-driven switching for $\beta=0°$, 10°, and 30° [(a) LR $\rightarrow$ HR at $I=4.8$ mA; (b) HR $\rightarrow$ LR at $I=-3.8$ mA]. Our simulations show that the reversal process and the switching times for $\beta=10°$ and $\beta=30°$ are similar to each other and are similar to those pre-

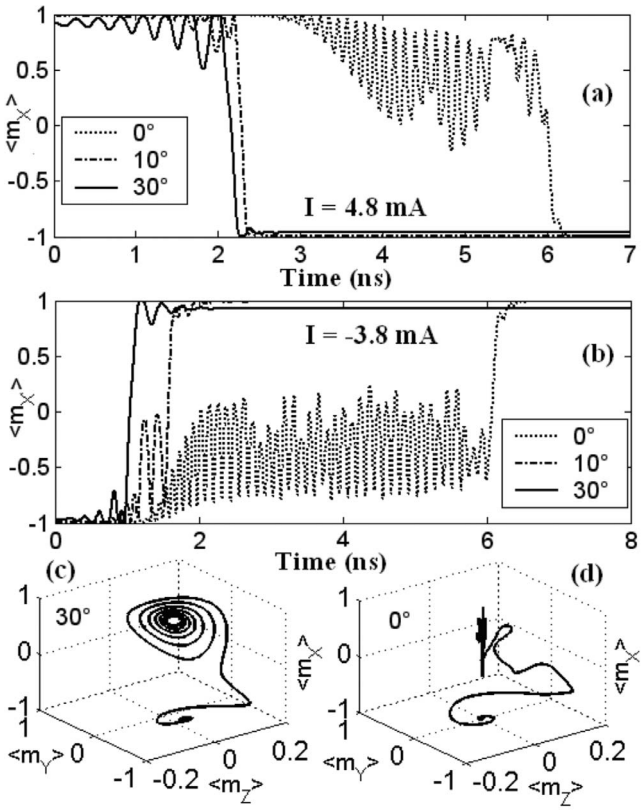

FIG. 1. Temporal evolution of the x component of the magnetization for three initial offset angles between the pinned and free magnetic layers (β=0°, 10°, and 30°). (a) LR→HR reversal; (b) HR→LR switching. Bottom: trajectories of the average magnetization during LR→HR reversal for (c) β=30° and (d) β=0°.

dicted by the macrospin model of magnetization reversal,[10] which are in agreement with experimental measurements.[3,11] That is, for β=10° and β=30°, we observe precession with increasing amplitude followed by a fast switching for all switching events, as can be seen in the trajectory reversal for β=30° [Fig. 1(c)]. Inspection of the magnetization during the reversal process shows that the state of magnetization is close to the macrospin state throughout the reversal process [Fig. 2 (top left and right)] whenever $\beta > 5°$.

However, we find that the zero-temperature switching time for β=0° increases dramatically compared to that for $\beta > 5°$. Concurrently with the increase in the switching time, a change of the reversal mechanism takes place. For β=0°, the reversal occurs via a complex nucleation process. Prior to complete reversal, stages with different magnetization dynamics can be distinguished. Initially, there is small-amplitude oscillation of the magnetization at the tips of the ellipse (0–2 ns), then an oscillation zone can be seen (2–6 ns) in which a vortex nucleates and moves across the sample (Fig. 2, center left, t_1=5.27 ns), giving rise also to a complex domain configuration (Fig. 2, center right, t_2=6 ns), before finally the reversal is accomplished. A similar process of vortex-nucleated magnetic reversal was predicted by Ref. 4 for a $150 \times 100 \times 2$ nm^3 elliptical $Co_{86}Fe_{14}$ nanomagnet with β=0°.

The reason for the change of the magnetization reversal process can be understood qualitatively by considering the

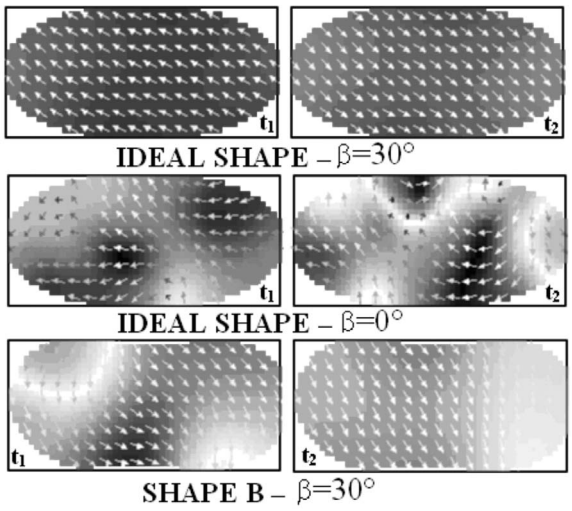

FIG. 2. Snapshots of the magnetization configuration during the reversal processes shown in Figs. 1 and 3. Top: ideal shape with β=30° at t_1=0.93 ns and t_2=1.35 ns. Center: ideal shape with β=0° at t_1=5.27 ns and t_2=6 ns. Bottom: shape B (see Fig. 3) with β=30° at t_1=1.38 ns and t_2=1.67 ns.

magnitude and direction of the spin-transfer torques in the cases of β=30° and β=0°. Since the magnitude of spin torque is roughly proportional to $\sin(\beta)$, in the case of β=30°, the spin torque acting on each spin of the free layer is relatively large and the variations from one micromagnetic cell to another are small. This situation of, a large, nearly uniform spin torque leads to a nearly coherent rotation of all spins of the free layer and gives rise to the coherent precessional reversal of the magnetization. For the case of β=0, the spin torque acting on each micromagnetic cell is small and can vary in direction because the micromagnetic state of the free magnetic layer differs from a uniform polarization. The trajectory of the moment for β=0 [Fig. 1(d)] can therefore be irregular during the initial stages of the reversal process, and spatially nonuniform magnetization patterns can develop such as those shown in Fig. 2 (center, ideal shape with β=0°). In addition, since the spin torque magnitude is initially small when β=0°, the Oersted field due to applied current can play a more important role in the initial stages of the reversal process.[12] Since the Oersted field has a circular symmetry, it promotes the development of a vortex state, as shown in Fig. 2 (center). Because the initial magnitude of the spin torque is small for the β=0°, T=0 case, there is a long (2–3 ns) initial stage in the reversal process in which only small changes of the magnetic state of the system are observed. However, as will be shown in Sec. III, this slow initial stage is generally eliminated by thermal fluctuations at temperatures as low as a few kelvin.

Our conclusions regarding the effect of the equilibrium angle between the magnetizations of the pinned and free layer on current-driven magnetization dynamics are similar to those recently published in Ref. 13.

Next, we consider the issue of nonideal sample shapes. To our knowledge, all reported micromagnetic simulations of current-driven excitations of magnetization in nanoscale spin valves have been performed for idealized shapes. However,

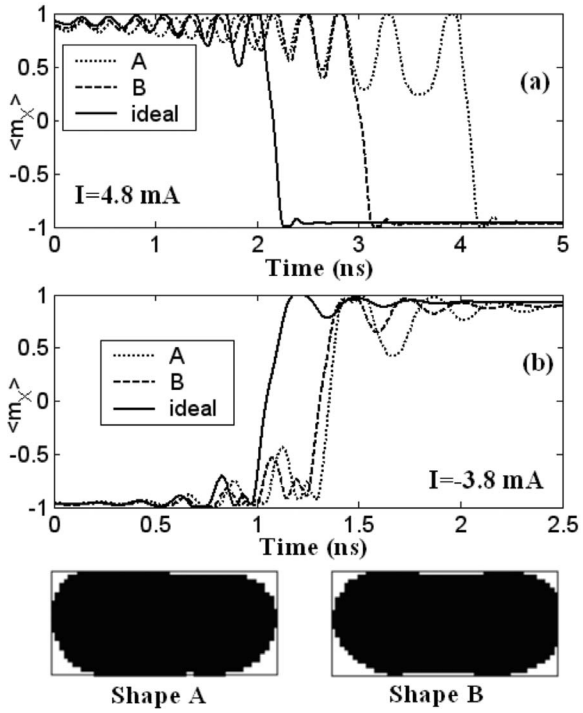

FIG. 3. Temporal evolution of the x component of magnetization for an ideal ellipse and two nonideal shapes (A and B) for $\beta=30°$. (a) LR→HR switching; center: (b) HR→LR switching. Bottom: the nonideal shapes used for performing our simulations.

real nanoscale samples exhibit substantial imperfections. The extent of validity of simulations for ideal sample shapes for the description of real current-induced magnetization dynamics has not been examined previously.

Figure 3 shows the temporal evolution of the x component of the free-layer magnetization for an ideal ellipse and for two nonideal shapes (shapes A and B) [(a) LR→HR transition at $I=4.8$ mA; (b) HR→LR at $I=-3.8$ mA, $\beta=30°$]. The nonideal shapes are computed from scanning electron microscopy (SEM) images of nanopillars with elliptical cross sections similar to those used in the experiment.[3] In order to obtain the discretized nonideal shapes with a size similar to the ideal shape, we assign the larger linear dimension of the SEM image the value of 130 nm, while the smaller dimension is assigned the value of 60 nm (these values are close to the actual dimension of the SEM image). Then, we use an algorithm which approximates the SEM images using square cells of 2.5×2.5 nm^2.

Our simulations reveal that nonidealities can change the reversal time and produce some increase in the spatial inhomogeneity of the magnetization during the reversal process. However, nucleation of a vortex does not take place for shapes A and B for $\beta=30°$. Figure 2 (bottom) shows snapshots of magnetization during the HR→LR reversal for shape B at $t_1=1.38$ ns and $t_2=1.67$ ns. The spins initially rotate in a spatially coherent way. After approximately 1 ns, the spins at the left and right edges of the nanomagnet begin to precess faster than those in the central part. A complete reversal then follows, without the creation of a vortex state.

We have performed detailed studies of the effect of shape nonideality on the reversal process using a number of different sample shapes. The results show that the reversal time can either increase or decrease depending on the type of deviations from the ideal elliptical shape and that in some cases, the reversal mechanism can be different from the quasicoherent rotation shown in Fig. 2 (bottom) (e.g., we find that edge defects can act as centers for domain wall nucleation). Our main conclusion is that while simulations of the current-induced magnetization reversal process performed for ideal sample shapes can give qualitative estimates of the switching time, they should not be trusted to give precise quantitative predictions for real systems. Nevertheless, regardless of the shape imperfections, the dominant factor determining the reversal mechanism for large current pulses is the misalignment angle β between the free and pinned layers.

We now compare the results of our micromagnetic simulations to experimental data obtained for the same sample geometry [exchange-biased 130×60 nm^2 $Ir_{20}Mn_{80}$ (8 nm)/Py (4 nm)/Cu (8 nm)/Py (4 nm) elliptical spin valves] used in the simulations. To mimic the experimental situation, in the simulation, the pinned layer is exchange biased in the plane of the sample at an angle of 45° with respect to the major axis of the ellipse, with an effective exchange field of 75 mT. We numerically solved the static LLG equation[6] for the entire spin valve ($Ir_{20}Mn_{80}$/Py/Cu/Py) structure. Due to the combined effects of exchange biasing, shape anisotropy, and magnetostatic coupling between the pinned and the free layers, the misalignment angle between the free and fixed layer magnetizations in the stable static configuration is $\beta\sim30°$. Because we expect that the presence of the antiferromagnet should increase the magnetic damping of the pinned layer by 1 order of magnitude compared to the free layer,[14] we assume in the dynamic simulations that the magnetization of the pinned layer is time independent.

We include thermal effects[15,16] in our simulations in order to study the effect of temperature on the reversal process and to make direct comparison to temperature-dependent experimental data. We add a random thermal field $\mathbf{h}_{th}$ (a randomly fluctuating three-dimensional vector) to $\mathbf{h}_{eff}$ for each micromagnetic cell. We assume that the fluctuating field is independent of the spin torque and that the magnetization configuration of the pinned layer does not depend on temperature.[16,17] Each component of $\mathbf{h}_{th}$ has the magnitude $(\xi/M_s)\sqrt{2(\alpha k_B T_S/\mu_0\gamma_0\Delta V M_s\Delta t)}$, where k_B is the Boltzmann constant, ΔV is the volume of the computational cubic cell, Δt is the simulation time step, T_S is the true temperature of the sample,[16,17] and $\boldsymbol{\xi}$ is random numbers from a Gaussian distribution with zero mean and unit variance.[15] Due to Joule heating, the temperature of the sample can be higher than the background substrate temperature (T_B). In the experiment, the degree of heating was estimated by comparing the temperature dependence of the resistance $R(T_B)$ in the absence of current to the dependence of the dc resistance on current $R(I)$ at a fixed temperature (see Ref. 18 for details). Of the temperatures considered in our simulations (7, 40, 120, and 240 K), heating should be very significant only at 7 K, and for this value to a good approximation, the experiments indicate $T_S=T_B+C_I|I|$ with $C_I=5$ K/mA.

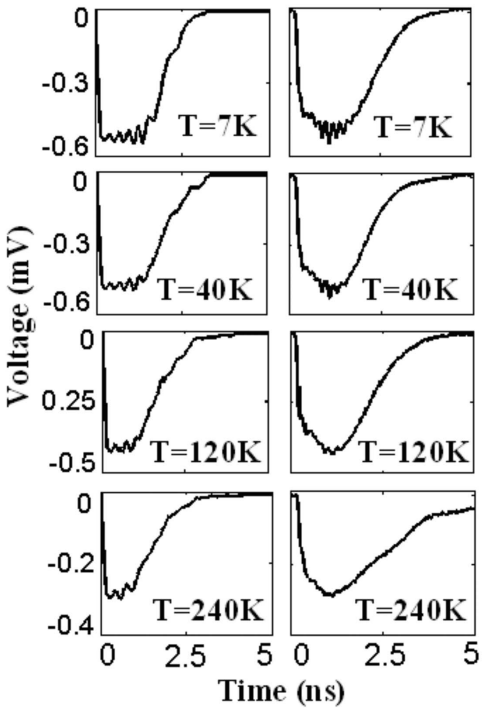

FIG. 4. A comparison between computed (left) and experimentally measured (right) voltage signals due to current-induced magnetization reversal from the low- to the high-resistance state for $\beta=30°$ at four background temperatures (7, 40, 120, and 240 K) and a current of 4.8 mA.

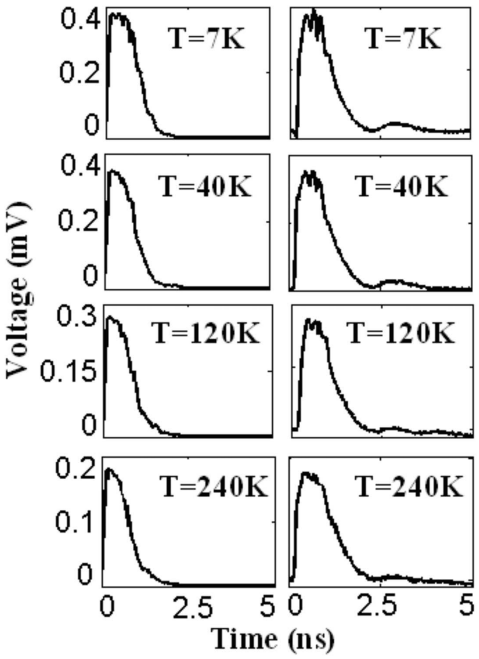

FIG. 5. A comparison between computed (left) and experimentally measured (right) voltage signals due to current-induced magnetization reversal from the high to the low resistance state for $\beta=30°$ at four background temperatures (7, 40, 120, and 240 K) with a current of −3.8 mA.

To enable comparison with the experimental data reporting statistical averages, we calculate the variation of the sample resistance with time, $R(t)$, over 50 switching events and then average. The initial state of the magnetization of the free layer was assumed to be slightly different for each switching event. These initial states were obtained by calculating the time evolution of the magnetization using the LLGS equation (including thermal effects with different random seeds) with zero applied current for 4 ns.

The right panels of Figs. 4 and 5 show experimental data for the current-induced reversal of magnetization between the two stable static states of the free layer—the LR and the HR states of the spin valve. Each plot is an average over 20 000 sampling oscilloscope traces. The abscissa axis for the plots is the time after application of a current step to the device. For Fig. 4 (right panels), the ordinate axis is the difference between the voltage measured for a LR→HR reversal and the voltage measured for the same current pulse applied to the sample initially in the high-resistance state, for which switching does not occur (it is a LR→HR process). The experimental voltage signal is therefore approximately $V(t)=|I(t)|\ (R(t)-R_f)$, where $I(t)$ is the current through the spin valve, $R(t)$ is the time-dependent resistance of the spin valve, and $R_f \equiv R(t\rightarrow\infty)$ is the value of resistance of the sample after reversal. The initial drop of the voltage signal in Fig. 4 in the time interval of ~150 ps is due to the finite rise time of the current step $I(t)$ applied, and it is not related to any substantial change in the magnetic state of the device. After the current step is fully turned on, the negative voltage in Fig. 4 corresponds to the low-resistance state of the device. As a function of time, the magnetization of the free layer starts precessing, as indicated by oscillations of the voltage signal (and therefore the sample resistance). The amplitude of oscillations increases with time. After the amplitude of oscillations becomes large, the free-layer nanomagnet switches from the low- to the high-resistance state, corresponding to zero voltage at large times. Figure 5 (right panels) shows the analogous voltage differences for a HR→LR reversal. Note that in both Figs. 4 and 5, the amplitude of the voltage signal $V(t)$ decreases with increasing temperature. This is due to the temperature dependence of the GMR effect.

The experimentally measured voltage signals in Figs. 4 and 5 are obtained by a stroboscopic technique employing a broadband sampling oscilloscope and thus are averages over many switching events.[3] Due to thermal fluctuations induced by the nonzero temperature of the sample, the magnetic trajectories and the reversal time will vary from one switching event to another. As a result of averaging over a distribution of switching times, the transition between the low- and high-resistance states appears to be gradual, spanning a time interval of about 1 ns.

The left panels of Figs. 4 and 5 show the computed signals for the LR→HR transition and HR→LR transition at the four background temperatures employed in the experiment (50 switching events were used in each simulation). The quantities χ and P in the expression for spin torque were used as fitting parameters to match the experimentally measured ensemble-average switching times for the LR→HR and HR→LR reversal processes at the background tempera-

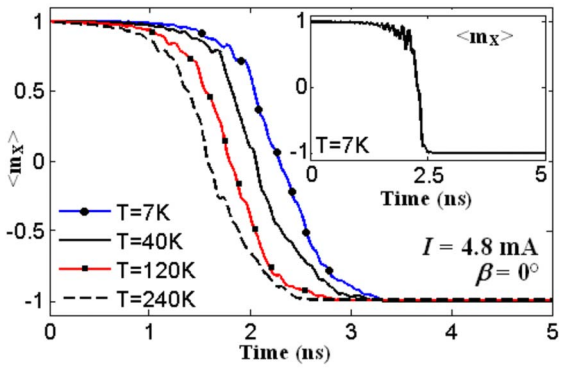

FIG. 6. (Color online) Temporal evolution of the x component of the magnetization for LR→HR reversal for $\beta=0°$ at four background temperatures (7, 40, 120, and 240 K), averaged over 50 iterations. Inset: temporal evolution of the x component of the magnetization for a single iteration of a LR→HR reversal for a background temperature of 7 K.

ture of 7 K. This fitting procedure gives unique values of χ and P because χ mainly influences the difference between the two switching times, while P mainly controls their average. The values of the fitting parameters obtained are $\chi=1.5$ and $P=0.38$. These values should be considered approximate estimates rather than quantitatively precise because, as noted above, the average reversal times can be altered by nonidealities in the shapes of real samples.

Detailed quantitative agreement between our experimental and simulated results should also not be expected because our simulations do not take into account the temperature dependence of a number of important parameters such as the spin current polarization, the magnetization, and the Gilbert damping.[19] Nevertheless, our simulations for $V(t)$ robustly reproduce the main qualitative features of the experimental data: (i) the gradual transition between low- and high-resistance states (this gradual transition is caused by averaging over many more-abrupt switching events at different times), (ii) the increase as a function of temperature in the widths of the simulated LR→HR and HR→LR transitions (and thus in the dispersion of switching times), and (iii) the decrease of the amplitude of oscillations of $V(t)$ with increasing temperature (this decrease is explained by the dephasing of oscillations induced by thermal fluctuations of the magnetization).

For an ideal shape and $\beta=30°$, the thermal effects do not change the macrospinlike precessional reversal mechanism observed at zero temperature. Similarly, for an ideal shape and $\beta=0°$, micromagnetic simulations including the thermal effects ($T_B=7$, 40, 120, and 240 K) show that the switching mechanism occurs via a nucleation process and does not change qualitatively compared to that at 0 K. However, in contrast to the case of $\beta=30°$, where the reversal time is only weakly dependent on the background temperature, in the case of $\beta=0°$, thermal fluctuations significantly decrease the switching time (see Fig. 6). This is because thermal fluctuations effectively eliminate the long (~2.5 ns) initial stage of the reversal observed at $T=0$ K (Fig. 1), which involves motion of magnetization with very small amplitude around its equilibrium configuration. Thermal fluctuations introduce significant misalignments between the magnetizations of the free and pinned layers, which increase the magnitude of spin torque and reduce the reversal time of each individual switching event (inset Fig. 6) with respect to the 0 K case. The results of our simulations for $\beta=0°$ show that the average reversal times for LR→HR reversal at $T_B=7$ and 240 K are 2.75 and 1.9 ns, respectively, substantially shorter than the $T=0$ K switching time of 6.0 ns. Furthermore, these switching times are only moderately longer than those calculated at the same temperatures for the case of $\beta=30°$, as can be seen by comparing the time responses in Figs. 4 and 6.

IV. CONCLUSIONS

In conclusion, we have compared micromagnetic simulations to experimental data for spin-torque-driven magnetic reversal and have found good qualitative agreement. The simulations demonstrate that for current pulses significantly larger than the zero-temperature critical current for switching, the key factor determining the mechanism of magnetization reversal is the equilibrium angle between magnetizations of the free and pinned layers. We find that in the case of collinear magnetizations for the pinned and free layers ($\beta=0$), current-induced magnetization reversal proceeds via a complex process involving a vortex nucleation. However, even relatively small misalignments of magnetizations of the pinned and free layers (>50°) lead to a dramatic change of the reversal mechanism, giving a coherent precessional reversal process similar to that assumed in macrospin models. The switching time decreases by about a factor of 3 when the equilibrium angle between the pinned and the free layers increases from 0° to 10°. The inclusion of a nonzero temperature in the simulations leads to a broadening of the distribution of reversal times in good agreement with the experimental data. However, at temperatures exceeding a few kelvin, the reversal times for $\beta=0°$ and $\beta=30°$ are found to be similar.

Perhaps most importantly, we find that the perfectly collinear configuration of magnetizations of the pinned and the free layers—the geometry most commonly used in micromagnetic simulations—is anomalously sensitive to small perturbations of the sample geometry, including thermal fluctuations, the influence of the Oersted field, changes in the misalignment angle, and changes in sample shape.

ACKNOWLEDGMENTS

The authors are grateful to Anna Giordano for software support. Work at Cornell was supported by the Office of Naval Research and the National Science Foundation's Nanoscale Science and Engineering Centers program through the Cornell Center for Nanoscale Systems. We also acknowledge NSF support through use of the Cornell Nanoscale Facility node of the National Nanofabrication Infrastructure Network and the use of the facilities of the Cornell Center for Materials Research.

[1] J. A. Katine, F. J. Albert, R. A. Buhrman, E. B. Myers, and D. C. Ralph, Phys. Rev. Lett. **84**, 3149 (2000); J. Grollier, V. Cros, H. Jaffres, A. Hamzic, J. M. George, G. Faini, J. B. Youssef, H. Le Gall, and A. Fert, Phys. Rev. B **67**, 174402 (2003); M. AlHaj-Darwish, H. Kurt, S. Urazhdin, A. Fert, R. Loloee, W. P. Pratt, Jr., and J. Bass, Phys. Rev. Lett. **93**, 157203 (2004); T. Devolder, C. Chappert, P. Crozat, A. Tulapurkar, Y. Suzuki, J. Miltat, and K. Yagami, Appl. Phys. Lett. **86**, 062505 (2005); S. Kaka, M. R. Pufall, W. H. Rippard, T. J. Silva, S. E. Russek, J. A. Katine, and M. Carey, J. Magn. Magn. Mater. **286**, 375 (2005); R. H. Koch, J. A. Katine, and J. Z. Sun, Phys. Rev. Lett. **92**, 088302 (2004); B. Oezyilmaz, A. D. Kent, D. Monsma, J. Z. Sun, M. J. Rooks, and R. H. Koch, *ibid.* **91**, 067203 (2003).

[2] M. Tsoi, A. G. M. Jansen, J. Bass, W. C. Chiang, M. Seck, V. Tsoi, and P. Wyder, Phys. Rev. Lett. **80**, 4281 (1998); S. I. Kiselev, J. C. Sankey, I. N. Krivorotov, N. C. Emley, R. J. Schoelkopf, R. A. Buhrman, and D. C. Ralph, Nature (London) **425**, 380 (2003); M. Covington, M. AlHajDarwish, Y. Ding, N. J. Gokemeijer, and M. A. Seigler, Phys. Rev. B **69**, 184406 (2004); W. H. Rippard, M. R. Pufall, S. Kaka, S. E. Russek, and T. J. Silva, Phys. Rev. Lett. **92**, 027201 (2004).

[3] I. N. Krivorotov, N. C. Emley, J. C. Sankey, S. I. Kiselev, D. C. Ralph, and R. A. Buhrman, Science **307**, 228 (2005).

[4] Y. Acremann, J. P. Strachan, V. Chembrolu, S. D. Andrews, T. Tyliszczak, J. A. Katine, M. J. Carey, B. M. Clemens, H. C. Siegmann, and J. Stöhr, Phys. Rev. Lett. **96**, 217202 (2006).

[5] J. Miltat, G. Albuquerque, A. Thiaville, and C. Vouille, J. Appl. Phys. **89**, 6982 (2001); K. Lee, A. Deac, O. Redon, and J. Nozieres, Nat. Mater. **3**, 877 (2004); D. V. Berkov and N. L. Gorn, Phys. Rev. B **72**, 094401 (2005); **71**, 052403 (2005).

[6] J. Slonczewski, J. Magn. Magn. Mater. **159**, L1 (1996); **195**, L261 (1999).

[7] L. Lopez-Dıaz, L. Torres, and E. Moro, Phys. Rev. B **65**, 224406 (2002); L. Torres, L. Lopez-Dıaz, E. Martınez, and O. Alejos, IEEE Trans. Magn. **39**, 2498 (2003); L. Torres, L. Lopez-Diaz, E. Martinez, M. Carpentieri, and G. Finocchio, J. Magn. Magn. Mater. **286**, 381 (2005). Our micromagnetic code has been tested with the standard problem of Micromagnetic Modeling Activity Group (http://www.ctcms.nist.gov/~rdm/mumag.org.html).

[8] J. Slonczewski, J. Magn. Magn. Mater. **247**, 324 (2002).

[9] G. Bertotti, *Hysteresis in Magnetism* (Academic, New York, 1999).

[10] J. Z. Sun, Phys. Rev. B **62**, 570 (2000).

[11] F. B. Mankoff, R. D. Dave, N. D. Rizzo, T. C. Eschrich, B. N. Engel, and S. Teherani, Appl. Phys. Lett. **83**, 1596 (2003).

[12] D. Apalkov, M. Pakala, and Y. Huai, J. Appl. Phys. **99**, 08B907 (2006); G. Finocchio, M. Carpentieri, B. Azzerboni, L. Torres, E. Martinez, and L. Lopez-Diaz, *ibid.* **99**, 08G522 (2006).

[13] M. D. Stiles and J. Miltat, in *Spin Dynamics in Confined Magnetic Structures III*, Springer Series Topics in Applied Physics Vol. 101 (Springer-Verlag, Berlin, 2006).

[14] P. Lubitz, M. Rubinstein, J. J. Krebs, and S. F. Cheng, J. Appl. Phys. **89**, 6901 (2001).

[15] W. F. Brown, Jr., Phys. Rev. **130**, 1677 (1963); J. L. Garcia-Palacios and F. J. Lazaro, Phys. Rev. B **58**, 14937 (1998); D. M. Apalkov and P. B. Visscher, *ibid.* **72**, 180405(R) (2005).

[16] I. N. Krivorotov, N. C. Emley, A. G. F. Garcia, J. C. Sankey, S. I. Kiselev, D. C. Ralph, and R. A. Buhrman, Phys. Rev. Lett. **93**, 166603 (2004).

[17] Z. Li and S. Zhang, Phys. Rev. B **69**, 134416 (2004).

[18] I. N. Krivorotov, D. V. Berkov, N. L. Gorn, N. C. Emley, J. C. Sankey, D. C. Ralph, and R. A. Buhrman, Phys. Rev. B **76**, 024418 (2007).

[19] N. C. Emley, I. N. Krivorotov, O. Ozatay, A. G. F. Garcia, J. C. Sankey, D. C. Ralph, and R. A. Buhrman, Phys. Rev. Lett. **96**, 247204 (2006).